A&A 448, 1061–1073 (2006)
DOI: 10.1051/0004-6361:20041754

Astronomy & Astrophysics

Hydrodynamic simulations of the accretion disk in U Geminorum

The occurrence of a two-armed spiral structure during outburst

M. Klingler

Mathematisches Institut der Universität Tübingen, 72076 Tübingen, Germany
e-mail: klingler@na.uni-tuebingen.de

Received 25 June 2003 / Accepted 11 October 2005

ABSTRACT

Aims. We use a new numerical hydrodynamic technique to simulate the evolution of the disk in 2D until the outburst is fully developed. The results are used to construct Doppler tomograms that closely agree with the time-resolved spectroscopic observations of U Geminorum during its 2000 March outburst when it showed two spiral arms.
Methods. We use the Shakura-Sunyaev alpha viscosity prescription for the disk, where most of the angular momentum transport originates in internal stresses rather than in globally excited waves or shocks. Other effects, such as the Rossby-waves instability found in axisymmetric potentials, are often found discussed as a possible cause of angular momentum transport. These Rossby-waves also show a spiral pattern, but most of them may be damped out due to the viscous hydrodynamic assumption. Our simulations reproduce the spiral feature that was found in the observational data, which confirms the eligibility of the so-called α-disk model. Radiation transport in the vertical direction is taken into account by solving the energy equation, while the calculations consider dissipative heating and radiative cooling with adequate opacity laws.
Results. We found that the outburst of U Geminorum can be described within the "disk-instability-model", as the viscous stress lets the disk expand out to regions where tidal disturbances induce a two armed spiral pattern. Initially these arms first become optically thick and then they get hot. A heating wave propagates until the whole disk is optically thick. In this state the two-armed spiral pattern still exists, and its spatial location is strongly correlated with the location of the two stars. This is in excellent agreement with those observations showing two transient spirals during outburst. A high resolution calculation of the region surrounding the hot spot is given in this paper. We examine whether the physical conditions near the hot spot – or near the inner boundary layer – are suitable for inducing thermal instability.

Key words. hydrodynamics – instabilities – accretion, accretion disks – binaries: close – stars: dwarf novae – stars: individual: U Geminorum

1. Introduction

Dwarf novae (DNe) are a subgroup of cataclysmic variables (CVs), which are close binaries with mass transfer from the secondary to the primary star. The donor, a low-mass, late-type main sequence star, fills its Roche lobe and loses mass to the accretor, a white dwarf (WD). The lost mass is collected in an accretion disk around the primary star. Accretion disks are found in close binaries when the magnetic field strength of the primary star can be neglected, which is the case in U Gem. The lost mass undergoes dissipative processes, which leads to a loss of potential energy. This energy is radiated away, and the mass flow ends in an accretion process on the surface of the WD. In dwarf novae, the loss of this energy is high enough to make the accretion disk the dominant part of the optical light curve during outburst. U Gem is the prototype of a Dwarf Novae, where the extinction along the line of sight is low. It has been the subject of many observations and UV investigations, such as the one by Long et al. (1993) and the references therein.

The theoretical nature of these dissipative processes in the disk is poorly understood. An often-favored mechanism is turbulence driven viscosity. We follow this approach by using the α-disk model of Shakura & Sunyaev (1973) in our calculations. In such models, the evolution of the disk is governed by the viscous stress and gravitational forces, while pressure forces are weak in the approximation of a thin accretion disk. Other sources of viscosity may be caused by spiral waves or may be shock-driven by the gravitational perturbation of the secondary (Savonije et al. 1994). It is known that, in the case of tidal waves, the $m = 2$ mode (two spiral waves) is the most unstable. Heemskerk (1994) investigated different components of the tidal potential with regard to the origin of the spiral formation. Newer investigations take either Rossby-wave instabilities into account to explain the high amount of angular momentum transport (Li et al. 2000) or large eddy simulations, and these two are also possible in axisymmetric potentials; see e.g. Godon & Livio (1999).

Hydrodynamic simulations are generally able to reproduce such instabilities, but one must keep in mind that the viscous approach in the calculation might damp out some of these effects. This is especially true for artificial viscosity, which is needed in most hydrodynamical computations to resolve strong shocks in the accretion disks, since the gas flow is highly super sonic. Even if tidally induced spiral shocks are unimportant for the angular momentum transport budget, they could still exist in an outburst. However, they can be reproduced with viscous hydrodynamical computations. Recently, it has been demonstrated that the origin of turbulence and angular momentum transport in accretion disks is very likely related to a linear, local, magnetohydrodynamic (MHD) instability – the magnetorotational instability; see Balbus & Hawley (1991) and the review by Balbus & Hawley (1998). In these models, the MHD instability is the origin of turbulence, while the turbulence itself sustains the magnetic field. This mechanism is efficient enough to account for angular momentum transport in weakly ionized disks, too. MHD simulations result in a different spatial distribution of turbulence and local dissipation. A comparison of the α-disk model and the MHD instability model is given too in Balbus & Hawley (1998). Future MHD simulations could help to work out the influence of the MHD approach itself and of some uncertain parameters, e.g. the rate of ioniziation or the conductivity of the disk matter.

Nonetheless, in this essay we compare simulations of the evolution of accretion disks with the observed data of U Gem during its outburst in March 2000 (Groot 2001). Our aim is to verify if the viscous disk simulations are consistent with the observed spiral structure. It seems that there has been a discrepancy between 2D simulations and 3D simulations in the past, with the 2D simulations unable to reproduce the observation for the regime of temperature expected in disks in CVs; see e.g. Godon et al. (1998). Future numerical parameter studies and additional observational input may provide new constraints on angular momentum processes as well as helpin determining the dominant physics in accretion disks.

For our simulations, we use a new numerical hydrodynamical method, the FINITE MASS METHOD (FMM) developed by H. Yserentant (see Gauger et al. 2000). This technique is a gridless, Lagrangian method for compressible fluids, and a short introduction will be given in the next section.

Even though theoretical studies imply instabilities in the accretion flow, the detection of instabilities in the simulations does not guarantee their existence in reality. The instabilities might only occur in the discrete (numerical) model and not in the continuous model, though vice versa the numerics mostly do not reproduce all instabilities that are possible in the continuous problem. Comparing the results using different hydrodynamical methods seems very beneficial in this discussion. A well-known method to simulate accretion disks in CVs is the "Smoothed Particle Hydrodynamics" (SPH). Armitage & Murray (1998) use SPH to simulate an outburst of IP Pegasi. In this context, our work has to be understood as an additional numerical input in the interpretation of computational results. To our knowledge the simulation of an outburst in U Gem using FMM has not been done yet. A short comparison to the SPH results is also given in this article.

1.1. The thermal instability model in accretion disks

The dwarf nova U Geminorum is known to undergo outbursts on timescales between 30 and 250 days (Warner 1995). The duration of an outburst amounts approximately to 15 days and its magnitude is ~4.5 mag according to Groot (2001). The most favored model to explain a dwarf novae outburst is the so-called disk instability model (DIM). In this model the thermal instabilities, triggered by the ionization of matter, cause the local heating of the disk; see e.g. Meyer & Meyer-Hofmeister (1981). Such outburst models have been studied in great detail (e.g. Ludwig et al. 1994, and references therein). The most remarkable statement concerning this DIM is that the balance between the mass transfer rate, or rather the viscosity, and the surface mass density is not definite. The existence of two stable and one unstable solutions gives the shape of an "s-curve" to this mathematical function.

The theoretical explanation for the outburst phenomenon is that it is a cyclic change of the disk structure between a hot, optically thick and a cool, optically thin state. Here, the treatment of the kinematic viscosity parameter ν plays a central role. In the α-disk model, ν is proportional to the sound speed c_s and the scale height H of the disk. The scale height describes the equilibrium between pressure forces and gravitational forces in the z-direction, perpendicular to the disk plane. In this case, the parameter ν is a function of the two independent thermodynamic quantities, the surface density Σ, and the Temperature T; additionally, ν is a function of the gravitational potential of both stars. The α-disk model now introduces the additional dimensionless parameter α with the assumption $0 < \alpha \leq 1$. The free choice of this parameter reflects ignorance of the real physical conditions in the disk. Multiple treatments of α can be found in the literature; α can be constant (Lin et al. 1985; Meyer & Meyer-Hofmeister 1989), constant with different values in the cold and the hot state (Smak 1984; Cannizzo et al. 1986), as well as time-dependent (Cannizzo 1993) or dependent on H, $\boldsymbol{x}$, and c_s (Duschl 1989; Meyer & Meyer-Hofmeister 1984).

In our computations, we consider a globally constant α. We run two separate simulations with $\alpha = 0.05$ and $\alpha = 0.5$. The choice of an overall constant α avoids additional assumptions on the viscosity model that are theoretically badly motivated. Our aim is to test if an outburst could be triggered only by considering the suitable opacity laws.

When the density and temperature in the disk reach some critical values, the matter ionizes and the disk becomes optically thick, heats up, and the hot branch in the s-curve is reached. In this state, more energy is lost due to radiation. Though the matter is optically thick, the strong T^4 dependence of the black-body radiation overbalances. The supplementary energy is provided by a higher accretion rate that comes from a higher viscosity. If we keep α constant, the kinematic viscosity ν depends on Σ and linearly on T.

One dimensional analytical investigations (Meyer & Meyer-Hofmeister 1989,e.g.) lead to the prediction that the higher mass transfer rate in the hot state, assuming α to be constant, is insufficient to explain the outburst cycle. With our intention of doing high resolution 2D simulations, we cannot

compute entire outburst cycles until more computational resources are available.

One consequence of the present shear viscosity in the accretion disk is a flattening of any density structures. Any local peak in the density profile will be completely smoothed out under the influence of shear viscosity. This effect is amplified by the α-parametrization of the viscosity, because the kinematic viscosity parameter increases with higher surface density and higher temperatures. All this leads to a fast depletion of dense regions of the disk in axisymmetric models or 1D simulations. Still this result could be compensated for by the tidal disturbance of the secondary, if the full Roche-potential is considered. Mass could then flow from regions with lower density and lower viscosity into hotter and denser regions. This procedure causes mass to accumulate in some preferred regions, thereby forming two spiral arms. At these regions the outburst will finally start.

Our simulation starts with an empty disk and ends at a state where nearly all parts of the disk are in the hot branch. The depletion of the disk is not computed. The observed duration of the outburst amounts to approximately 15 days, a duration that corresponds to ~15 000 Keplerian orbits of a test particle around the primary at the innermost simulation radius.

Our work include a high spatial-resolution computation of the "hot spot", the region where the in-falling gas stream interacts with the outer rim of the disk. We find out that this region never reaches the hot branch. The hot spot is optically thin and bright, but the temperature is lower than the temperature in those regions of the accretions disk that reached the hot branch. In recent works the hot spot is renamed the "bright spot", which could answer the question of whether the bright spot is the predominant trigger for an outburst. Still, our results imply that this is not likely. In the case of U Gem, the bright spot occurs in a region far away from the primary and secondary. In this region the gravitational forces, perpendicular to the disk plane, are not strong enough to compress the matter up to ionization. This property is possibly changed in other binaries with a closer separation or a different mass ratio.

The second region, one that is potentially able to trigger the thermal instability, is the boundary layer at the inner radius near the WD. Gravitational forces compress the gas, and the high velocity of the viscous gas flow dissipates more energy. A correct treatment of this region, in which the gas is finally accreted on the surface of the primary, requires a high spatial resolution in 3D and is not performed in our simulation. Some theoretical aspects of the boundary layer are worked out by Popham et al. (1993) and Godon et al. (1995). The smallest simulation radius r_i is less than half of $r_{\min}$, which is the closest distance to the primary that a free falling test mass could reach, starting from the inner Lagrangian point L_1 with zero velocity. In an early state of the outburst, particles located at r_i also reach the hot branch. This happens only a few orbital periods after the outburst starts in the two spiral arms. Hence, these particles have the ability to heat up particles in their neighborhood and to induce a heating wave that could expand over the entire disk. In our simulation, we find out that the velocity of this heating wave is very slow compared to the development of the outburst in the outer regions. As long as the boundary layer at the white dwarf is not highly resolved, it is not clear whether the hot branch is first reached at the innermost radius or in the outer spiral arms, but it seems to be the case that these regions do not influence each other. Both outburst regions expand independently at first and join each other later at a radius that is approximately 2−3 times $r_{\min}$. In these observations, the spiral arms are presented immediately after the outburst has started.

2. Modeling of the accretion disk in U Geminorum

The parameters of U Gem are given, for example, by Warner (1995). The masses of the white dwarf and the secondary are $M_1 = 1.15\,M_\odot$ and $M_2 = 0.67\,M_\odot$, while the mass ratio is defined as $q = M_2/M_1$. The orbital period is $\Omega = 15\,285$ s, and the separation of the two stars a. The position of the center of mass is (CM). We assume Keplerian law and circular orbits. The mass transfer rate is $\dot{M} = 10^{-9}\,M_\odot/\mathrm{yr}$. These values are not known exactly, and other sources give different values; see Froning et al. (2001) and the references therein. Our simulations show that the infalling gas stream and the hot spot have no influence on the evolution of the outburst (see 3.3). Therefore, the mass transfer rate has only a minor influence on the outburst cycles; however, we are not investigating this process here. The role of the other parameters, such as the star masses, should be elaborated in future simulations based on this work. We choose the CM as the origin of our coordinate system. All simulations are done in the co-rotating frame of the binary. The secondary is located at $x < 0$ and the primary at $x > 0$. The external forces acting on the gas are described by the Roche potential, which includes the gravitational forces of both stars and centrifugal forces. In addition, we consider velocity-dependent Coriolis forces.

2.1. Input parameters for the in-falling gas stream

Our simulation starts with an empty disk. In a small region near L_1, we give analytical input parameters for the in-falling gas stream and let the accretion disk develop self-consistently. The principal hydrodynamic conditions near the L_1-point are studied in great detail in Lubow & Shu (1975). The basic parameters for the accretion stream are mass ratio q and scaling parameter

$$\epsilon = \frac{c_s(T_2)}{a\Omega}. \tag{1}$$

This is the ratio of the isothermal sound speed at the surface of the secondary and the orbital velocity of the system. For the surface temperature of the secondary, we choose $T_2 = 6000\,\mathrm{K}$. We make use of the following fitting functions for the vertical (H_s) and horizontal (W_s) scale heights of the stream, which are given by Hessmann (1999) and are functions of q, a, and the distance to the white dwarf R:

$$H_s(R,q,a) \approx h_1(R/a)\cdot h_2(q)\cdot a\epsilon \tag{2}$$

$$W_s(R,q,a) \approx w_1(R/a)\cdot w_2(q)\cdot a\epsilon \tag{3}$$

with the polynomial fits

$$h_1(R/a) = 0.06 + 3.17\frac{R}{a} - 2.90\left(\frac{R}{a}\right)^2 \tag{4}$$

$$w_1(R/a) \;=\; 0.084 + 3.09\frac{R}{a} - 3.08\left(\frac{R}{a}\right)^2 \tag{5}$$

to h_1 and w_1 and the power-law fits

$$h_2 \;=\; 0.89\, q^{-0.11} \tag{6}$$

$$w_2 \;=\; 0.90\, q^{-0.15}. \tag{7}$$

For the velocity

$$V_\mathrm{s}(R, q, a) \equiv v_\mathrm{s}(R/R_{L_1})\,\sqrt{2GM_1/R_{L_1}}, \tag{8}$$

we use the parametrization

$$v_\mathrm{s}(r_L) = 1.87 - 1.87\, r_L + 4.1 \cdot \exp(-r_L/0.085) \tag{9}$$

with $r_L = R/R_L$. These are good approximations for $0.05 \le q \le 0.5$, which holds for the binary U Gem. The angle between the x-axis and the gas stream in the co-rotating frame (see Lubow & Shu 1975) is

$$\cos(2\theta) = -4/(3A) + \sqrt{1 - 8/9A} \tag{10}$$

with

$$A = \frac{\mu}{\left|R_{L_1}/a - 1 + \mu\right|^3} + \frac{1-\mu}{\left|R_{L_1}/a + \mu\right|^3} \tag{11}$$

and

$$\mu = \frac{M_2}{M_2 + M_1}. \tag{12}$$

The setup of the accretion stream is as follows. In a square near the L_1-point with the x-coordinates

$$L_{1,x} + 0.05 \cdot d_{LW} \le x \le L_{1,x} + 0.1 \cdot d_{LW}, \tag{13}$$

where d_{LW} is the distance from L_1 to the white dwarf, we give a constraint to the thermodynamic quantities, which are the velocity field $v(\boldsymbol{x}, t) = v_\mathrm{s}$, the temperature $T(\boldsymbol{x}, t) = T_2$, and the surface density Σ. As density profile we choose a Gaussian distribution centered on a line with angle θ intersecting the x-axis at the L_1-point. The central density of the stream ρ_s is easily obtained by integrating the density of the stream over the widths and heights while conserving mass:

$$\rho_\mathrm{s} = \dot{M}/(2\pi W_\mathrm{s} H_\mathrm{s} V_\mathrm{s}). \tag{14}$$

We find that the simulated trajectory of a free-falling test mass agrees well with the parametrization of the velocity field. In our coordinates, the binary is rotating counter-clockwise, so the infalling gas stream near the L_1-point has positive v_x and negative v_y.

2.2. The hydrodynamic model of the disk with α-viscosity

Given the constraint in the region near the L_1-point, the accretion disk can develop according to the hydrodynamic laws of an ideal gas. We use a constant adiabatic exponent $\gamma = 5/3$ and a constant mean molecular weight $\mu = 0.5$ u (u is the atomic mass unit) for ionized hydrogen. We neglect the self-gravity of the disk, radiation pressure, heat conduction, and radiative transfer in the disk plane. We then follow the usual approximations for thin disks, given for example in Frank et al. (1992). The disk height H describes the ratio of pressure forces and gravitational forces perpendicular to the disk plane. Here H is given by

$$H = c_\mathrm{s}/\Omega_K \tag{15}$$

where Ω_K is the angular velocity of a test mass on a Keplerian orbit around its central mass. In the case of the binary we consider both stars, $\Omega_K = \Omega_{K1} + \Omega_{K2}$, where H determines the relation between the density ρ and the surface density Σ integrated over the disk height

$$\rho = \Sigma/H. \tag{16}$$

As discussed, we choose the α prescription for the kinematic shear viscosity parameter

$$\nu = \alpha c_\mathrm{s} H \tag{17}$$

with the constant, dimensionless parameter α.

To solve the energy equation of the gas, we consider the radiative cooling rate per unit surface area and per side of the disk

$$D \;=\; \frac{4\sigma}{3\tau} T_\mathrm{c}^4 \tag{18}$$

where σ is the Stefan-Boltzmann constant and τ the optical depth of the disk. The heating rate Q_+ includes the energy production by viscous dissipation and dissipation in shocks. In the numerical case, shock dissipation is resolved by additional artificial viscosity or friction terms that are discussed later. The optical depth of the disk is given by

$$\tau = \kappa_R \Sigma \tag{19}$$

with the opacity $\kappa_R = \kappa_R(\rho, T_\mathrm{c})$. For the mean Rosseland opacities, we use the power-law fits given by Bell & Lin (1994), see Fig. 1. The fits cover a wide range of temperatures $1\text{–}10^6$ K, and they consider electron scattering, bound-free and free-free transmission, H-scattering, and the existence of molecules. The most important region in our simulations is the one between 10^4 and 10^5 K, as there is a strong increase in κ_R due to ionisation.

Using the relations (15) to (19) the functions ν, D, and Q_+ can be expressed in terms of the entire set of hydrodynamic field quantities $\Sigma(\boldsymbol{x}, t)$, $T_\mathrm{c}(\boldsymbol{x}, t)$, and $\boldsymbol{v}(\boldsymbol{x}, t)$.

2.3. The numerical method

By using the Finite Mass Method (FMM) we determine the evolution of the disk. This method is based on concepts developed by Yserentant (1997, 1999a,b) and are described in detail by Gauger et al. (2000). Still, only a short description of the main principles, namely its behavior and its features, will be given in this essay.

The FMM is a gridless Lagrangian particle method to solve problems in compressible fluid dynamics. Particle methods are suitable in connection with astrophysical hydrodynamics, particularly when open boundary conditions appear. In addition,

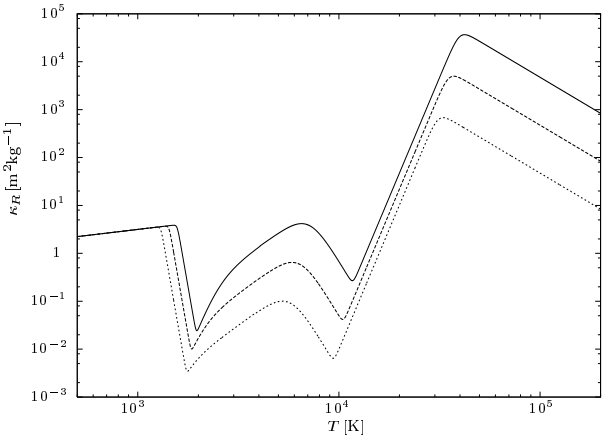

Fig. 1. The opacities are functions of temperature and density. The different curves correspond to different densities, *from top to bottom*: $\rho = 10^{-4}, 10^{-5}$ and 10^{-6} kg m^{-3}. The strong increase between 10^4 K and 10^5 K is caused by the ionization. Note the double logarithmic scaling.

the Lagrangian assumption is advantageous when considering supersonic flows.

In contrast to finite element or finite volume methods, FMM is based on a discretization of mass and not of space. These mass packets move under the influence of internal and external forces and the laws of thermodynamics. They can intersect and penetrate each other. The particles can have individual masses m_i and specific entropies S_i. The set of all particles approximates the density $\rho(\boldsymbol{x}, t)$ and entropy density $s(\boldsymbol{x}, t)$. The approximation produces differentiable functions and not discrete quantities. We choose cubic B-splines for the internal mass and entropy distribution of a particle in one dimension. The higher dimensional shape function is built up by a tensor product-like assumption that has good approximation properties. The initial set of particles, arranged on a uniform grid, approximates the functions ρ and s up to fourth order.

For our simulations, we use the 2D version of FMM. The approximated density is now interpreted as the surface density Σ of the disk, i.e. the integrated density over the disk height H. The same argument holds for the entropy.

The dependent thermodynamic quantities, i.e. the central temperature T_c in the disk plane and the pressure P are expressed as functions of Σ and s by using the Gibbs fundamental relation of thermodynamics and an expression for the internal energy of a barytropic ideal gas. With the assumption of an adiabatic, inviscid flow, we use the internal energy of the gas as potential energy and derive the motion for the particles from a Lagrange function.

The particles can move independently. The movement of a 2D particle has six degrees of freedom, two for the translation and four for a linear deformation of the internal shape function. The particles can change their size in each direction, then can rotate and undergo shear. Due to the deformation feature, the set of all particles yields a second-order approximation of the true velocity field. Without this feature only first order would be obtained. The second-order convergence of the method is shown for flows in a given velocity field or for flows solely driven by external forces (see Yserentant 2000). This stable behavior of the method allows us to simulate a differentially rotating accretion flow in Cartesian coordinates. In test simulations of accretion disks with an axisymmetric potential, the particles are set on an equally spaced Cartesian grid. In these test simulations, there is no pattern of the initial grid in the resulting density after a few rotations of the disk. The deformation of the particles has to follow the differentially rotating flow. They are deformed to sharp needles tangentially to the trajectory. In such a situation it is necessary to stop the integration, to smooth the fields by applying a low pass filter, and then to replace them by a new set of particles. In the context of FMM, this procedure is called "restart" and is described in detail in Gauger (2000). The restart procedure conserves the second order approximation of the velocity field. The dissipation of momentum and energy is negligible: the dissipated energy during the restart procedure is more than three magnitudes less than the heat generation caused by the α-viscosity.

To damp the fluctuation of the local kinetic energy, additional frictional forces are applied to the particles. These forces are vanishing in the limit of particle sizes tending to zero. Still, these forces are linear in the velocity difference $R(\boldsymbol{v}_i - \boldsymbol{v})$ where $\boldsymbol{v}_i$ is the velocity approximated by the particle i of interest, $\boldsymbol{v}$ the velocity approximated by all particles (including the i-th particle), and R is the frictional parameter that can depend on thermodynamical quantities. However, R stays a constant value in our calculations. These frictional forces are important for resolving shock fronts where dissipation in inviscid fluids occurs. The dissipated energy leads to a generation of entropy that we consider in the energy equation. In shock-tube test-simulations, we observe that the friction forces do not produce a flattening of the shock fronts, as they usually do when using artificial viscosity like the von Neumann-Richtmyer viscosity (von Neumann & Richtmyer 1950). Artificial viscosity mostly depends on the trace of the velocity derivative. Its effect shows similarities to the physical bulk viscosity like the flattening of shock fronts. However, we have to keep in mind that the outlined frictional forces also act, if all derivatives of the velocity are zero. Without the occurrence of a shock the force above described softly gathers the particles together.

The accretion flow in U Gem is highly supersonic. Strong shocks occur in the disk itself, but mainly in the region of the hot spot. The good behavior of FMM in resolving these shocks now becomes adverse as it leads to stiff equations. Therefore, we introduce an additional numerical viscosity that is similar to a physical bulk viscosity in smoothing strong shocks. Furthermore, we increase the time step.

Interestingly, some similarities between FMM and the Smoothed Particle Hydrodynamics method (SPH) (see Monaghan 1992) can be spotted in the following way. When we remove four degrees of freedom for an FMM particle, so that deformations are no longer possible, and give these particles a spherical internal mass distribution, as well as a reduction of the space integration to a one-point formula, we should obtain the SPH formulation. In the SPH, the space integration is often called SPH-sum. However, the one point integration formula is the sum over the particles itself. With respect to the higher approximation order of FMM, a multi point integration formula

is generated for each particle matching to the chosen spline as shape function.

We use the time-stepping scheme described in Gauger et al. (2000). This is basically the Störmer-Verlet method with an additional Krylov subspace approximation for the velocity dependent forces. If we consider the full energy equation with radiative cooling, it leads us to very stiff equations and requires an additional operator splitting step.

This cooling term step solves the equation

$$\frac{\partial T}{\partial t} \propto T^4, \tag{20}$$

and we obtain the new local temperature T_1 of a part of the disk with initial temperature T_0 after the time Δt as

$$T_1 = \left[\frac{8\sigma}{\tau \Sigma c_v} \Delta t + T_0^{-3} \right]^{-\frac{1}{3}} \tag{21}$$

where σ is the Stefan Boltzmann constant. To solve the energy equation, we subdivide each dynamical time step into 300 sub-steps $\Delta\tilde{t}$, each of which contains a heating and a cooling part. The heating procedure is an explicit Euler step with a constant heat supply, following the viscous and frictional dissipation. The cooling step is given in Eq. (21). We are now able to update the function

$$\tau = \tau\left(\kappa(\tilde{t}), \Sigma(t)\right) \tag{22}$$

for each sub-step, which means an update of κ in the sub-steps $\Delta\tilde{t}$. By using enough sub-steps, we can reach the situation the alternating heating and cooling procedures each cover a temperature range ΔT that is small compared to an average temperature $\bar{T}$ of the disk. We find out that for 300 sub-steps

$$\Delta T < 10^{-4} \bar{T} \tag{23}$$

can be reached. Surprisingly the approximation of a constant heat supply for all sub-steps fits the real physical conditions in the disk. The dynamical time step is about the same order as the time a sound wave with isothermal sound speed would need to traverse the disk height H. Keeping H constant locally during the sub-steps, which means keeping α and also the viscous dissipation constant, agrees with the interpretation of viscosity in the α-model.

3. Simulations

In the previous section we described how we determine the initial conditions in the region near the L_1 point. Our simulations start with an empty disk. The first 20 orbital periods are simulated without solving the energy equation, therefore, a polytropic assumption for the gaseous matter is now used instead. At this time, a small and nearly axisymmetric disk has established itself. With the described restart procedure we are able to change the spatial resolution in our simulations. Matter has to accumulate in the disk for a few hundred binary orbits before an outburst starts. We carried out such a simulation with a small number of particles. A few orbits before the outburst starts we increase the particle number. The spatial resolution per dimension now is 250 or 330 particles. In the simulation area, which exceeds the Roche lobe radius by approximately 30%, a maximum of 40 000 particles are active.

During the restart procedure, particles that have left the simulation area will be dropped. The mass of the particles passing the accretion radius $R_{wd} = 0.022\,a$ (a is the binary separation) are then understood to be accreted onto the primary. With this procedure we simulate an open boundary condition where mass can leave the simulation area but cannot come back in. This corresponds to the behavior of open boundary conditions in hydrodynamical grid codes.

In the following figures, the surface density Σ, the radiative energy loss D, and the optical depth τ in different states of the disk are given. To produce the figures, we choose a regular Cartesian grid with 551×551 points. For each grid point, we specify the hydrodynamical field quantities Σ and s within the FMM context. This means that we sum over all particles that overlap the actual grid point. Using Eqs. (15) to (19) of our α-model, all other quantities can be computed in the positions of the grid points. The given pictures are obtained with a mapping of the functions onto a linear greyscale map where the minimum value, pictured by the color white, is always zero. The maximum value, given in black, is noted in the figure itself.

In all figures, the thin black line denotes the primary's Roche lobe. The tics on the x-axis are given for the center of mass (CM) and the white dwarf (WD). In the density pictures, the in-falling gas stream is not seen because its surface density is too low.

In the figures where the radiative energy loss is given, the fourth root of D is mapped to the greyscale map, but the maximum value is given for the quantity D itself. The first reason for this is to reduce the high contrast in function D and to obtain significant pictures. The second reason is the specification of a simple model to describe the monochromatic luminosity in the visible range of light. For the case of $h\nu/k_\mathrm{B}T \ll 1$, the Plank's black body radiation takes the Rayleigh-Jeans form and becomes proportional to the temperature

$$B_f(T) \propto f^2 T. \tag{24}$$

Therefore, we choose $D^{0.25}$ that is also proportional to the temperature. Observational velocity measurements are often done with visible light, e.g. with He II lines. The function $D^{0.25}$ is then proportional to the line intensity, if $T_\mathrm{c} \gg 6000\,\mathrm{K}$. The temperature in the disk exceeds this value almost everywhere.

In some figures a cut-of value is given for the function τ. The color black represents all $\tau \geq 100$. The resulting pictures show a high contrast, and the black regions give a good approximation of the sections where the disk is in the hot, optically thick state within the DIM. Note that function τ has a minimum value of 8/3 for both sides of the disk. This means that all radiation produced in the disk could escape directly. This minimum appears white on the print.

3.1. Disk structure in quiescence and during outburst

In Fig. 2 four states of an outburst are shown. Before the outburst starts the disk does not show any features of interest, and it is always nearly axisymmetric to the WD. At an arbitrary

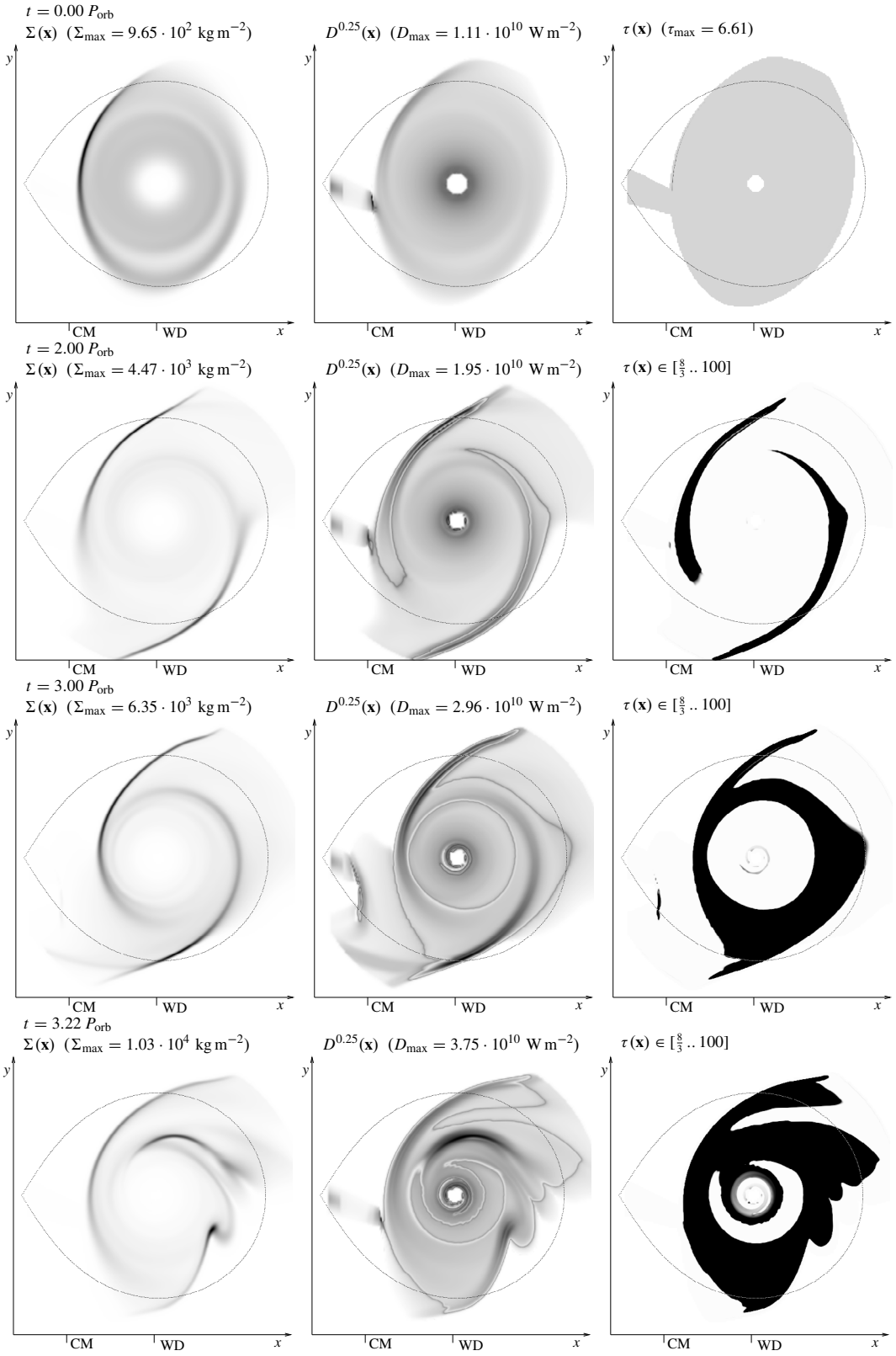

Fig. 2. Different stages of the outburst from the simulation with $\alpha = 0.05$. Shortly before the outburst starts (top row, $t = 0.0$), no significant spiral structures appear. Then the outburst starts forming two spiral arms ($t = 2.0$). One binary orbit later ($t = 3.0$), they are forming a ring, at this time a second ring at approximately $r = 0.07\,a$ reaches the hot branch. Both rings contact each other at time $t = 3.22$. The second (bottom right) spiral arm becomes instable. For further explanation see the text.

time, shortly before the outburst starts, we set the time equal to zero. This situation is given in the top row in Fig. 2. The total mass of the disk is 1.43×10^{20} kg, and the hottest and also brightest region is the hot spot with a maximum temperature of $T_c = 2.4 \times 10^4$ K. The disk now has an elliptical shape that exceeds the Roche lobe. Still, no significant spiral features can be detected. All sections of the disk are optically thin. In the figures of function D, the discontinuity of the in-falling gas stream near the L_1-point comes from the simulation technique. In this region the initial conditions are given as described above. After leaving this region, the matter cools down until it re-heats in the shock of the hot spot. In the figures of the functions D and τ, the in-falling gas stream seems to be very broad, but most of the mass is concentrated near the middle of the stream. The region marked grey denotes only the actual simulation area in which temperature and optical depth are defined.

Two binary orbits later, at time $t = 2.0$, the density profile has formed a two-armed spiral pattern. Both arms are relatively thin and strong, and both exceed the Roche lobe clearly. Around these arms, the disk reaches the hot branch and becomes optically thick, as seen in the figure of τ. At the boundaries of these optically thick regions, the conditions are suitable for high temperature and moderate optical thickness. Therefore, a high amount of radiation can escape at these boundaries and the shape of the function $D^{0.25}$ looks caldera like. Outside the roche lobe where the spirals are hot and the angular velocity is insignificant, the Mach number $M = v_\phi / c_s$ is small and comes close to the limit $M = 1$ of the thin disk approximation. In our simulations we found that $M > 1.7$ holds for the outer regions of the disk and that $M > 3$ holds for more than 96% of the disk mass.

At time $t = 3.0$, the spiral pattern and optically thick regions have formed an outer ring. The hot branch is also reached in an inner ring. Both rings come into contact at time $t = 3.22$. The last row shows a situation in which the second (lower right) spiral arm becomes unstable. The correlation with the ring contact may be coincidental. In later stages of the simulation, the second spiral arm is often unstable. In these states the whole disk is in the hot state. It seems as if its matter loses too much kinematic energy due to the higher viscosity in this spiral arm, and it begins to fall radially towards the WD. This procedure disturbs the disk structure strongly. Severe shocks in the disk are produced and a high amount of potential energy is converted into heat. A maximum temperature of $T_c = 1.76 \times 10^5$ K is detected at the time $t = 3.22$. While breaking down, the spiral arm melts and creats macroscopic vortices that are damped out after a short time due to our viscous approach. After this procedure, a new spiral arm forms. In our simulations, the first spiral arm (upper left) never becomes unstable.

3.2. The influence of the inner boundary layer

The previous results have shown that the outburst starts with the formation of two spiral arms in the outer regions of the disk. An open question is the role of the boundary layer at the surface of the WD. Maybe the conditions are appropriate to triggering an outburst. We do not present the 3D simulation necessary to verify this problem, but we can test the role of the boundary layer by imposing a new boundary condition. We do this with the following trick: at a suitable time we stop removing particles at the inner radius and the hole in the simulation area will be closed. To do this we must shorten the gravitational potential of the WD by multiplying the gravitational force with a reduction factor f_r

$$f_r = \left(\frac{r}{r_c}\right)^3 \quad \text{for} \quad r < r_c \quad \text{and} \quad f_r = 1 \quad \text{otherwise} \qquad (25)$$

and $r_c = 0.02\,a$. This leads us to an unphysical accretion at radius $r = r_c$, where the gas becomes optically thick very quickly. The function τ in Fig. 3 shows three rings: the innermost ring is the mass accreted unphysically, and the other rings are self-consistent solutions of the disk model. We did this simulation with a higher spatial resolution. The outburst develops in a slightly different way, so that the timescale does not fit the one from the simulation in Fig. 2 exactly. Our simulation shows that the outburst can start independently at the outer radius, by developing first two spiral arms which form a ring after some time, and at an inner radius. The outburst at the inner radius starts far away from the surface of the WD and is not induced or influenced by the boundary layer. We remind the reader that our model does not include heat conduction and radiation transport in the disk plane. If radiation in the radial and angular directions were included, the propagation of the ionization front from the inner disk and from the spiral arms would be even faster and more efficient. In boundary layer simulations, one uses the thin disk equations, together with a treatment of the radiation in the radial direction.

3.3. The influence of the hot spot

Here we consider whether the hot spot can trigger or affect the outburst. During the described restart procedure, we may change the resolution and magnify a part of the disk. From our simulation with $\alpha = 0.5$, we start with a disk in which the first spiral arm is developed. The region around the hot spot is then restarted with a refined particle mesh. We run the simulation for a time t that is four times as long as the time it takes for a free falling particle starting at the L_1-point to reach the hot spot. The resulting situation is shown in Fig. 4. We carry out this simulation without using the artificial bulk viscosity, but instead with the frictional terms. The FMM method is now able to reproduce very strong shocks that are much sharper than the shock occuring in the hot spot. We suspect the radiative energy loss might be responsible for the smoothing effect. We found in our simulation that the hot spot is bright compared to the spiral arms but not significantly hotter than them. Only a small region in the center of the hot spot is optically thick. This region does not grow, and it touches the other hot regions only at a later time. In our simulations, the hot spot plays no role with respect to the start of the outburst.

3.4. The influence of the viscous parameter α

In the Shakura-Sunyaev disk solution, the unknown parameter α does not enter any of the expressions for the disk

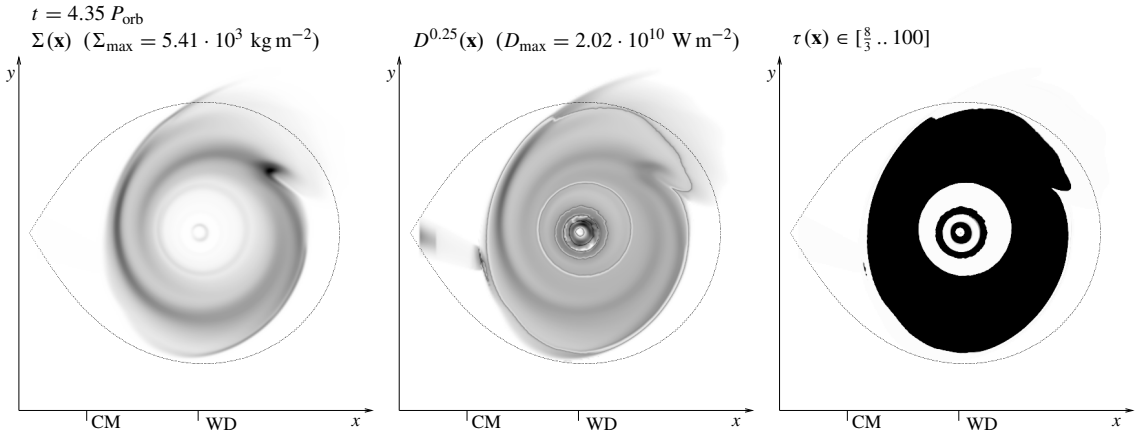

Fig. 3. Simulation with $\alpha = 0.05$. The potential of the WD is truncated and leads to an unphysical accretion at the innermost visible ring. The simulation is done with a higher resolution of 350×350 particles.

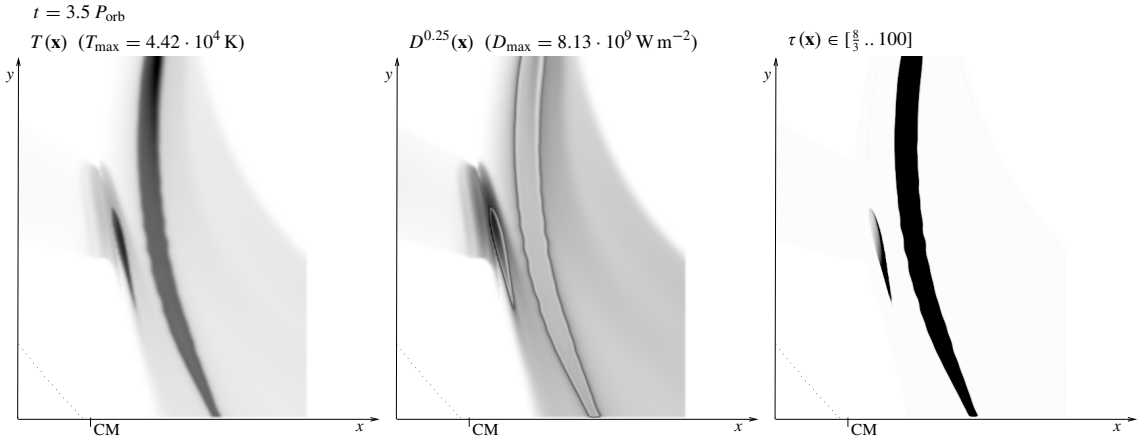

Fig. 4. Detail of the hot spot from the simulation with $\alpha = 0.5$. The first spiral arm has developed. The simulation is done with a higher local spatial resolution and without bulk viscosity. The hot spot is brighter, but not significantly hotter than the outburst spiral arms and does not influence or induce them. The resolution in the area shown is 348×348 particles.

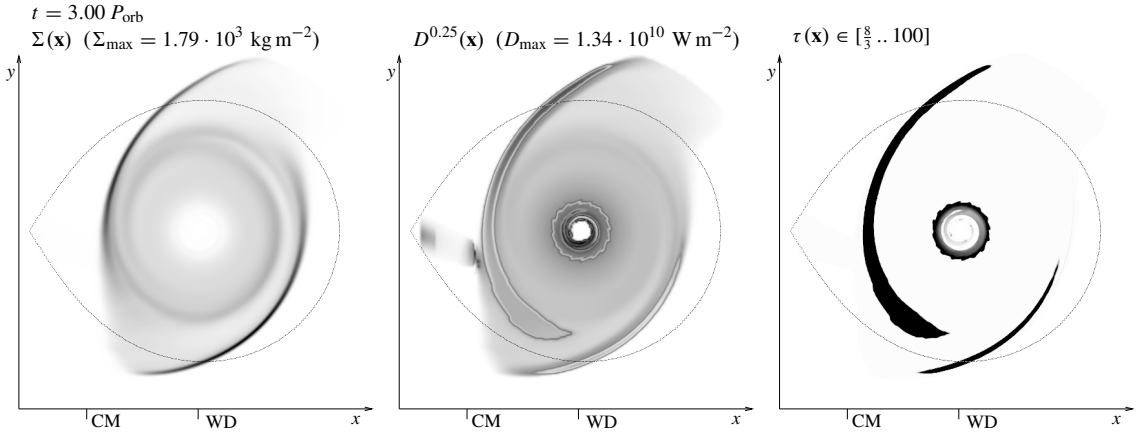

Fig. 5. The beginning of the outburst with $\alpha = 0.5$. The optically thick region around the second spiral arm is smaller and shows fluctuations. At a smaller radius, the outburst starts independently from the spirals.

quantities with a high power. We completed two simulations, one with $\alpha = 0.5$ and one with $\alpha = 0.05$. The results of these simulations lead to the same principal predictions concerning the phenomenon of the outburst. Only some varying details are noticeable. However, we will now issue only a qualitative description of the most important differences.

It is evident that simulations with different values of α will develop on different time scales; therefore, the offset of the time $t = 0$ cannot be compared in these two simulations. Figure 5 shows the disk in a state where the optically thick regions form a double spiral-arm pattern. This state is comparable to the state at $t = 2.0$ of the $\alpha = 0.05$ simulation given in the second row in

Fig. 2. The surface density of the two spirals shows a reduced variation, which means that a higher value of α leads to a fainter shock feature in the spirals. The two-armed spiral feature is closer to point symmetry relative to the WD's position and appears more upright in the co-rotating frame. The radius of the top left spiral is increased, while the other radius is decreased. In the $\alpha = 0.5$ simulation the top left spiral first reaches the optically thick state. One binary orbit later, the inner ring and the second spiral become optically thick simultaneously. While the second spiral appears stable in the surface density plot, the optically thick region around the second spiral is alternating in appearance between optically thick and one that is not so at all. These fluctuations iterate until the first spiral arm expands and finally surrounds the entire disk.

4. Doppler tomograms

Since no spatially resolved observations of interacting binary accretion disks are available, a successful method of observation for detecting any internal structure is the technique of Doppler tomography (Marsh & Horne 1988). The intensity of the observed spectral lines in this technique is obtained as the function of the flow velocity towards the observer and as a function of the binary phase ϕ, $f(v, \phi)$. If the emitting gaseous flow is assumed stationary in the rotating frame of the binary (and if the knowledge about the inclination is used), the spectral line profiles can be inverted to yield the best-fitting *Doppler map*, $I(v_x, v_y)$. In the *Doppler map* the line flux is given as a function of the velocity $\boldsymbol{v} = (v_x, v_y)$ in the observer's frame. The detection of spiral structure in U Gem by Groot (2001) is based on such a Doppler mapping method.

As shown in the previous section, function $D^{0.25}$ is a very sound approximation of the monochromatic line intensity in the range of visible light. Following the description below, we will evaluate the particle data on an equally spaced Cartesian grid. At each grid point, $\boldsymbol{v}(\boldsymbol{x})$ and $D^{0.25}(\boldsymbol{x})$ are evaluated. Then function $D^{0.25}(\boldsymbol{v})$ can be derived without the need of further assumptions.

Mapping into the velocity space is done as follows. Function $D^{0.25}(\boldsymbol{x})$ is evaluated on a very fine Cartesian grid with 2000×2000 points. Each grid point now represents a unique area of space. The velocities at these grid points are given by the simulated flow velocity and the added velocity of the co-rotating frame. For these points we also define a reasonable $\Delta\boldsymbol{v}$ so that all points represent a unique area in velocity space. Now we define an equally spaced grid in velocity space with the same $\Delta\boldsymbol{v}$ and the resulting resolution of 550×550 grid points. Each of the velocity cells of the space grid intersects some cells of the velocity grid with a well-defined fraction of its volume. The function $D^{0.25}$ is now summed over the velocity grid cells. In the sum, the fraction described above is used as a weight function. This procedure causes a smoothing in the resulting Doppler map. Therefore we need not smoothe with a Gaussian window function, which is a common, but in our view a less motivated, method.

The mapping from space to velocity coordinates is done in a fixed time-step. We should be able to reconstruct the distorted maps that arise if the emission is not stationary in the frame of the binary. Still, as the evolution of the spiral pattern is slow compared to the orbital time-scale, this procedure is not necessary.

An inherent effect of the Doppler mapping of accretion disks into the space of velocity is that those patterns with a large radius and with a lower velocity are visible in a higher contrast, while the contrast of the patterns with a small radius are less clear. The emitting gas at the pattern with the small radius flows with nearly Keplerian velocity and covers a wide range of velocity cells. Therefore, it is only seen as a grey background.

In the Doppler tomograms in Fig. 6 the three small pictures above all tomograms demonstrate the situation in spatial coordinates. The frame of the binary rotates counterclockwise. The spiral arm in the top left quadrant has a negative y-velocity and appears again as the lower spiral in the tomograms near the secondary's Roche lobe. A spiral pattern that is point-symmetric to the WD in spatial coordinates will lose its symmetry in velocity coordinates as we consider the velocity of rotation in the co-rotating frame. Four different tomograms are given, one for the disk in quiescence and three for the disk during outburst. The disk in quiescence corresponds to the situation given in the top row of Fig. 2. The outburst will start in less than one binary orbit later. The outer rim of the disk, flowing with lower velocity, is seen as the inner rim in velocity coordinates. It will replace the hot spot as the dominating feature of the tomogram. The situation in the second picture ($t = 2.0$) represents the situation from the 2nd row in Fig. 2. The two armed and asymmetric spiral features form the dominant part in the tomogram. The lower left tomogram ($t = 7.25$) comes from the simulation with $\alpha = 0.5$, which has developed on a different timescale. In the situation as shown, the outburst has reached the inner parts of the disk, but the two armed spiral on the outside still persists. The hot inner parts of the disk, highly emitting and flowing with high velocity, are hardly detectable in the tomogram. It is dominated again by the slower two spiral arms. The last figure at lower right ($t = 5.35$), again from the simulation with $\alpha = 0.05$, represents the most interesting situation. The outburst has spread over the entire disk apart from some outer regions. A new two-armed spiral feature is seen in the surface density and in the function $D^{0.25}$. This spiral lies completely in the hot, optically thick region. The pattern of the spiral is the dominant feature in the Doppler tomogram and is much brighter than the hot spot. Comparing these results with the observations of Groot (2001), we discovered the existence of an excellent agreement in the velocity range, slope, and asymmetry of the observed pattern.

An exact quantitative comparison between computations and observations would require a definition of the measurement of the spiral characteristics. The spirals in the simulation appear in a smaller radial range than in the data of the observation. To allow a fruitful discussion, we define the distance $d_{v,2}$ of the second spiral arm to the WD in velocity coordinates in a diagonal direction into the first quadrant, i.e. from the WD towards equal positive v_x and v_y. The results from our simulations are as follows: $d_{v,2}(t = 2.0) \approx 530\,\mathrm{km\,s^{-1}}$ and $d_{v,2}(t = 5.35) \approx 660\,\mathrm{km\,s^{-1}}$; the spirals at $t = 2.0$ appear at a larger radius than at $t = 5.35$, a fact that is also seen in spatial coordinates. From the given observed tomogram, we estimate this radius at $d_{v,2,\mathrm{obs}} \approx 650\,\mathrm{km\,s^{-1}}$.

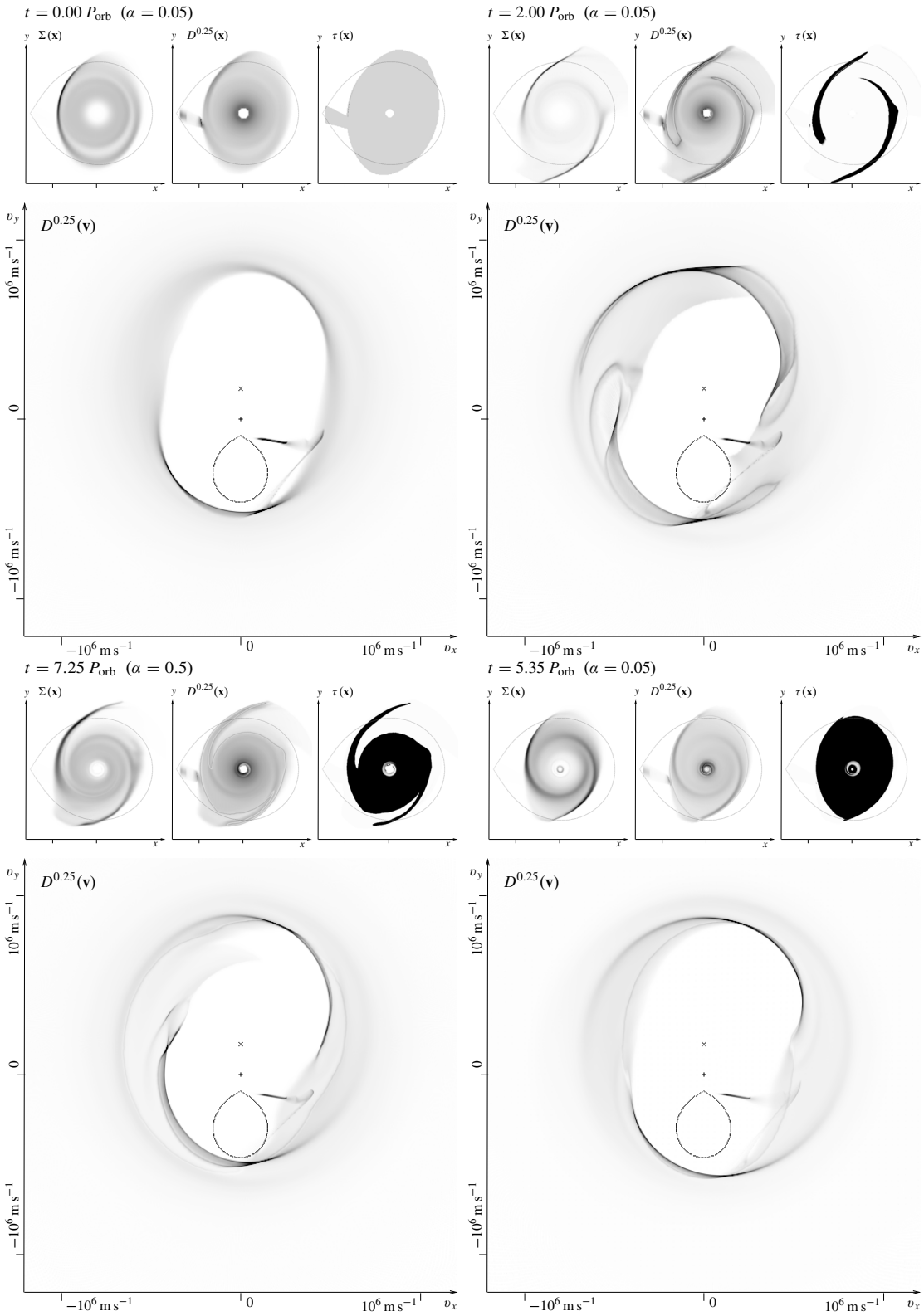

Fig. 6. Doppler maps from the simulation with $\alpha = 0.05$ at time $t = 0$, 2.0 and 5.35. The lower left map is from the simulation with $\alpha = 0.5$. The cross denotes the WD, the plus sign the CM and the "balloon" the secondary's Roche lobe. The diagrams above the Doppler maps show characteristic quantities as functions of the spatial coordinates.

At this point we would like to emphasize that all observational data are to be taken a few days after the outburst started. The duration of this outburst amounts to approximately 15 days. The most important result of our simulation is the fact that a few binary orbits (there are about 5.7 obits per day) after the outburst has started, the whole disk reaches the optically

thick state and stays there the next few orbits. Considering the timescale, only the tomogram computed at time $t = 5.35$ reproduces the situation in the data.

5. Discussion

This paper presents a simulation of the evolution of the accretion disk for the parameters of the binary U Gem in outburst. As our main result, we found that during the outburst the disk forms a two-armed spiral pattern, which is the dominant feature in the predicted Doppler tomograms. The spiral structure obtained in the simulation is stationary in the co-rotating frame and absent in quiescence. The main characteristics of the spiral pattern like slope, velocity range, and asymmetry are in excellent agreement with observations.

During certain stages of the outburst spiral, structures are formed. One stage ($t = 2.0$) shows two hot spirals, whereas the rest of the disk is cool and the appropriate Doppler agrees adequately with observations. This corresponds to the explanation of dwarf novae outbursts by Armitage & Murray (1998), who found similar spiral structures in the binary IP Peg using a simplified SPH code. Our simulations show that this situation lasts only for a short time. Therefore it seems improbable that this time range is included in the observations. Our simulations predict that the disk in outburst is hot and optically thick overall, apart from some outer regions. In this state the distribution of viscous stress becomes more homogeneous than in the intermediate stage shortly after the outburst starts. The viscous stress, considered within the α-model, causes the expansion of the disk to the tidal radius. The consequence of this expansion is a strong $m = 2$ mode that is excited during the outburst. This mode is stationary in the co-rotating frame and is seen in the data. The higher shear viscosity leads to a higher accretion rate onto the WD. The mass of the disk decreases, which will finalize the outburst.

Theoretical arguments suggest that quiescent disks are cool and do not spread to the tidal radius. This argument goes hand in hand with the observations of U Gem and other cataclysmic variables, as this research also could not find any evidence of spiral patterns in quiescent disks. Our simulations show that the quiescent disk is cool and optically thin and will reach the tidal radius shortly before the outburst starts.

By using the full 2D α-disk model with constant α in which no further input is required, the observations described above can be shaped accordingly. The outburst-triggering event is the strong increase of ionization at higher temperatures. This event can be computed with knowledge of atomic data. The correspondence between our simulations and the observed data is a sound confirmation of the α-model.

Our results show that the viscous approach can produce disks in which spiral shocks occur as well. Interestingly enough, this aspect corresponds to the conclusions of Savonije et al. (1994). In their research they discovered that the high amount of angular momentum transport found in the disks of cataclysmic variables could not be explained by the effect of spiral shocks. The turbulent shear viscosity in α-disks allows both angular momentum transport and spiral shock production.

More observations would be very useful, especially those that follow the formation of the first spirals of an outburst, as they would help us understand the interplay of factors modeling the angular momentum transport. Maybe some restrictions on the last free parameter α could be derived. Our simulations have shown that tidal forces lead to spirals, which are the event inducing the outburst within the DIM. Starting at these locations, the heating wave covers the whole disk. Additional triggering effects, like the hot spot or the inner boundary layer to the WD, do not seem to play an important role. Simulating multiple outburst cycles covering multiple months is an expensive project, as the typical timescales of radiation transport and flow dynamics are less than a second. Additional models for the boundary layer between the disk and the WD's surface could help to explain the total strength of the outburst as the boundary layer is likely to be an additional important radiative location. Other 3D effects may interact with the development of the outburst. Kunze & Speith (2001) have discovered that substantial stream-disk overflow interacts with the disk and can furthermore be observed as the absorption of X-rays.

We believe that the refinement of computer models and further observational input will lead to new and interesting insights into accretion physics. Therefore, we look forward to answering all the questions brought up in this essay, hopefully with the support of better and faster computers in the future.

Acknowledgements. The author wishes to thank the members of the TAT and CPT groups (theoretical astrophysics and computational physics in Tübingen) for their suggestions, due to their experience in astrophysical hydrodynamics using both SPH and grid codes. I also wish to thank the members of the NA group (numerical analysis in Tübingen) for providing and supporting new time integrators and finally the new finite mass method, which is parallelized using MPI. The simulations were done on the KEPLER-computer, a PC-cluster with Myrinet network provided by the SFB 382. This work was supported by the Deutsche Forschungsgemeinschaft (DFG) and is part of project C17 of the Sonderforschungsbereich SFB 382.

References

Armitage, P. J., & Murray, J. R. 1998, MNRAS, 297, L81
Balbus, S. A., & Hawley, J. F. 1991, ApJ, 376, 214
Balbus, S. A., & Hawley, J. F. 1998, Rev. Mod. Phys., 70, 1
Bell, K. R., & Lin, D. N. C. 1994, ApJ, 427, 987
Cannizzo, J. K. 1993, ApJ, 419, 318
Cannizzo, J. K., Wheeler, J. C., & Polidan, R. S. 1986, ApJ, 301, 634
Duschl, W. 1989, A&A, 225, 105
Frank, J., King, A. R., & Raine, D. J. 1992, Accretion Power in Astrophysics (Cambridge: Cambridge Univ. Press)
Froning, C. S., Long, K. S., Drew, J. E., Knigge, C., & Proga, D. 2001, ApJ, 562, 963
Gauger, C. 2000, Ph.D. Thesis, Eberhard-Karls-Universität Tübingen
Gauger, C., Leinen, P., & Yserentant, H. 2000, SIAM J. Numer. Anal., 37 No. 6, 1768
Godon, P., & Livio, M. 1999, ApJ, 523, 350
Godon, P., Livio, M., & Lubow, S. 1998, MNRAS, 295, L11
Godon, P., Regev, O., & Shaviv, G. 1995, MNRAS, 275, 1093
Groot, P. J. 2001, ApJ, 551, L89
Heemskerk, M. H. M. 1994, A&A, 288, 807
Hessmann, F. V. 1999, ApJ, 510, 867

Kunze, S., & Speith, R. 2001, MNRAS, 322, 499
Li, H., Finn, J. M., Lovelace, R. V. E., & Colgate, S. A. 2000, ApJ, 533, 1023
Lin, D. N. C., Papaloizou, J., & Faulkner, J. 1985, MNRAS, 212, 105
Long, K. S., Blair, W. P., Bowers, C. W., et al. 1993, ApJ, 405, 327
Lubow, S. H., & Shu, F. 1975, ApJ, 198, 383
Ludwig, K., Meyer-Hofmeister, E., & Ritter, H. 1994, A&A, 290, 473
Marsh, T., & Horne, K. 1988, MNRAS, 235, 269
Meyer, F., & Meyer-Hofmeister, E. 1981, A&A, 104, L10
Meyer, F., & Meyer-Hofmeister, E. 1984, A&A, 132, 143
Meyer, F., & Meyer-Hofmeister, E. 1989, A&A, 221, 36
Monaghan, J. J. 1992, ARA&A, 30, 543
Popham, R., Narayan, R., Hartmann, L., & Kenyon, S. 1993, ApJ, 415, L127
Savonije, G., Papaloizu, J., & Lin, D. 1994, MNRAS, 268, 13
Shakura, N. I., & Sunyaev, R. A. 1973, A&A, 24, 337
Smak, J. 1984, Acta Astron., 34, 161
von Neumann, J., & Richtmyer, R. D. 1950, J. Appl. Phys., 21, 232
Warner, B. 1995, Cataclysmic Variable Stars (Cambridge: Cambridge Univ. Press)
Yserentant, H. 1997, Numer. Math., 76, 111
Yserentant, H. 1999a, Numer. Math., 82, 161
Yserentant, H. 1999b, Numer. Math., 82, 143
Yserentant, H. 2000, SFB 382, Report Nr. 136